

Dimensional Crossover in 2D Crossbars

K. Kikoin, I. Kuzmenko, S. Gredeskul, Y. Avishai
Department of Physics, Ben-Gurion University of the Negev, Beer-Sheva
(October 23, 2018)

Spectrum of boson fields and two-point correlators are analyzed in quantum crossbars (QCB, a superlattice formed by two crossed interacting arrays of quantum wires), with short range inter-wire interaction. It is shown that the standard bosonization procedure is valid, and the system behaves as a sliding Luttinger liquid in the infrared limit, but the high frequency spectral and correlation characteristics have either 1D or 2D nature depending on the direction of the wave vector in the 2D Brillouin zone. As a result, the crossover from 1D to 2D regime may be experimentally observed. Plasmon propagation in arbitrary direction is possible. Periodic energy transfer between arrays ("Rabi oscillations") is predicted.

I. INTRODUCTION. FROM QUANTUM WIRES TO QUANTUM CROSSBARS

The behavior of electrons in arrays of 1D quantum wires was recognized as a challenging problem soon after the consistent theory of elementary excitations and correlations in a Luttinger liquid (LL) of interacting electrons in one dimension was formulated (see¹ for a review). One of the fascinating challenges existing in this field is a search for LL features in higher dimensions². Although the Fermi liquid state seems to be rather robust for $D > 1$, the possible way to retain some 1D excitation modes in 2D and even 3D systems is to consider highly anisotropic objects, in which the electron motion is spatially confined in major part of the real space (e.g., it is confined to separate linear regions by potential relief). One may hope that in this case weak enough perturbation does not violate the generic long-wave properties of the LL state. Arrays of interacting quantum wires may be formed in organic materials and in striped phases of doped transition metal oxides. Artificially fabricated structures with controllable configurations of arrays and variable interactions are available now due to recent achievements in nanotechnology (see, e.g.,³).

We start with a discussion of an array of parallel quantum wires. The conventional LL regime in a 1D quantum wire is characterised by bosonic fields describing charge and spin modes. We confine our discussion to the charge sector (LL in the spin-gapped phase). The Hamiltonian of an isolated quantum wire may then be represented in a canonical form

$$H = \frac{\hbar v}{2} \int_{-L/2}^{L/2} dx \left\{ g\pi^2(x) + \frac{1}{g}(\partial_x \theta(x))^2 \right\}. \quad (1)$$

Here L is the wire length, v is the Fermi velocity, θ, π are the conventional canonically conjugate boson fields and g is the dimensionless parameter which describes the strength of the interaction within the chain (see, e.g.,^{1,4}). The interwire interaction may transform the LL state existing in isolated quantum wires into various phases of 2D quantum liquid. The most drastic transformation is

caused by the *interwire* tunneling t_{\perp} in arrays of quantum wires with *intrawire* Coulomb repulsion. This coupling constant rescales towards higher values for strong interaction ($g < 1/2$), and the electrons in array transform into 2D Fermi liquid⁵. The reason for this instability is the orthogonality catastrophe, i.e. the infrared divergence in the low-energy excitation spectrum that accompanies the interwire hopping processes.

Unlike interwire tunneling, the density-density or current-current interwire interactions do not modify the low-energy behavior of quantum arrays under certain conditions. In particular, it was shown recently^{6–8} that an interaction of the type $W(n - n')$, which depends on the distance between wires n and n' but does not contain current coordinates x, x' , imparts the properties of a *sliding phase* to 2D array of 1D quantum wires. In this state an additional interwire coupling leaves the fixed-point action invariant under the "sliding" transformation $\theta_n \rightarrow \theta_n + \alpha_n$ and $\pi_n \rightarrow \pi_n + \alpha'_n$. The contribution of interwire coupling reduces to a renormalization of the parameters $v \rightarrow v(q_{\perp})$, $g \rightarrow g(q_{\perp})$ in the LL Hamiltonian (1), where q_{\perp} is a momentum perpendicular to the chain orientation. Such LL structure can be interpreted as a quantum analog of classical sliding phases of coupled XY chains⁹. Recently, it was found¹⁰ that a hierarchy of quantum Hall states emerges in sliding phases when a quantizing magnetic field is applied to an array.

In the present paper we concentrate on another aspect of the problem of interacting quantum wires. Instead of studying the conditions under which the LL behavior is preserved in spite of interwire interaction, we consider situations where the *dimensional crossover* from 1D to 2D occurs. In other words, we investigate regimes, where the excitations in quantum array demonstrate either 1D or 2D behavior in different parts of phase space. The most promising type of artificial structures where this effect may be expected is a periodic 2D system of two arrays of parallel quantum wires crossing each other at an angle φ . We call it "quantum crossbars" (QCB). The square grids of this type were considered in various physical context in early papers^{11–15}. In Refs.^{13,14} the fragility of the LL state against interwire tunneling in the crossing areas

of QCB was studied. It was found that a new periodicity imposed by the interwire hopping term results in the appearance of a low-energy cutoff $\Delta_l \sim \hbar v/a$ where a is a period of the quantum grid. Below this energy, the system is "frozen" in its lowest one-electron state. As a result, the LL state remains robust against orthogonality catastrophe, and the Fermi surface conserves its 1D character in the corresponding parts of the 2D Brillouin zone. This cutoff energy tends to zero at the points where the one-electron energies for two perpendicular arrays ϵ_{k_1} and ϵ_{k_2} become degenerate. As a result, a dimensional crossover from 1D to 2D Fermi surface (or from LL to FL behavior) arises around the points $\epsilon_{F_1} = \epsilon_{F_2}$.

We study this dimensional crossover for Bose excitations (plasmons) described by canonical variables θ, π in QCB. In order to unravel the pertinent physics we consider a grid with *short-range capacitive inter-wire interaction*. This approximation seems natural for 2D grids of carbon nanotubes³, or artificially fabricated bars of quantum wires with grid periods $a_{1,2}$ which exceed the lattice spacing of a single wire or the diameter of a nanotube. It will be shown below that this interaction can be made effectively weak. Therefore, QCB retains the 1D LL character for motion along the wires similarly to the case considered in Ref.⁸. At the same time, the boson mode propagation along some resonant directions is also feasible. This is essentially a 2D process in the 2D Brillouin zone of the reciprocal space.

II. QUANTUM CROSSBARS: BASIC NOTIONS

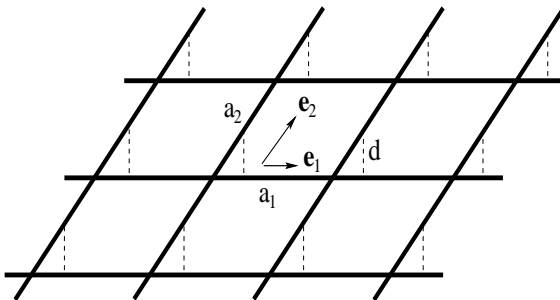


FIG. 1. 2D quantum bar formed by two interacting arrays of parallel quantum wires. Here $\mathbf{e}_1, \mathbf{e}_2$ are the unit vectors of the superlattice, a_1, a_2 are the superlattice periods and d is the vertical interarray distance

A quantum crossbars may be defined as a 2D periodic grid, i.e. two periodically crossed arrays of 1D quantum wires. In fact these arrays are placed on two parallel planes separated by an inter-plane distance d^3 , but in this section we consider QCB as a genuine 2D system. We assume that all wires of the j -th array, $j = 1, 2$, have the same length L_j , Fermi velocity v_j and Luttinger parameter g_j . They are oriented along unit vectors $\mathbf{e}_{1,2}$ with

an angle φ between them. Thus, the QCB periods along these directions are a_1 and a_2 , and the corresponding QCB basic vectors are $\mathbf{a}_j = a_j \mathbf{e}_j$ (Fig.1). The interaction between the excitations in different wires is assumed to be concentrated near the crossing points with coordinates $n_1 \mathbf{a}_1 + n_2 \mathbf{a}_2 \equiv (n_1 a_1, n_2 a_2)$. The integers n_j enumerate the wires within the j -th array. Such interaction imposes a superperiodicity on the energy spectrum of initially one dimensional quantum wires, and the eigenstates of this superlattice are characterized by a 2D quasimomentum $\mathbf{q} = q_1 \mathbf{g}_1 + q_2 \mathbf{g}_2 \equiv (q_1, q_2)$. Here $\mathbf{g}_{1,2}$ are the unit vectors of the reciprocal superlattice satisfying the standard orthogonality relations $(\mathbf{e}_i \cdot \mathbf{g}_j) = \delta_{ij}$. The corresponding basic vectors of the reciprocal superlattice have the form $(m_1 Q_1, m_2 Q_2)$, where $Q_j = 2\pi/a_j$ and $m_{1,2}$ are integers.

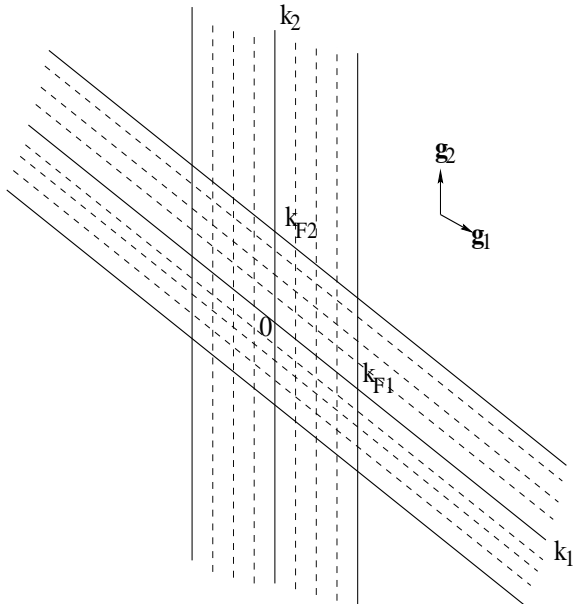


FIG. 2. Fermi surface of 2D metallic quantum bar in the absence of charge transfer between wires. $\mathbf{g}_1, \mathbf{g}_2$ are the unit vectors of the reciprocal superlattice

In conventional 2D systems, forbidden states in the inverse space arise due to Bragg diffraction in a periodic potential, whereas the whole plane is allowed for wave propagation in real space, at least till the periodic potential is weak enough. In strongly anisotropic QCB, most of the real space is forbidden for electron and plasmon propagation, whereas the Bragg conditions for the wave vectors are still the same as in conventional 2D plane modulated by a periodic potential. The excitation motion in QCB is one-dimensional in major part of the 2D plane, and the anisotropy in real space imposes restrictions on the possible values of the 2D coordinates x_1, x_2 ($\mathbf{r} = x_1 \mathbf{e}_1 + x_2 \mathbf{e}_2$). At least one of them, e.g., x_2 (x_1) should be an integer multiple of the corresponding array period a_2 (a_1), so that the vector $\mathbf{r} = (x_1, n_2 a_2)$ ($\mathbf{r} = (n_1 a_1, x_2)$) characterizes a point with a 1D coordinate x_1 (x_2) lying at the n_2 -th (n_1 -th) wire of the first

(second) array.

The 2D Brillouin zone of QCB is constructed as an extension of 1D Brillouin zones of two crossed arrays and subsequent folding of this BZ in accordance with the 2D superstructure. However, one cannot resort to the standard basis of 2D plane waves when constructing an eigenstate with a given wave vector \mathbf{k} in the BZ because of the kinematic restrictions mentioned above. Even in *non-interacting* arrays of quantum wires the 2D basis is two sets of 1D waves. These are 1D excitations propagating along each wire of array 1 characterized by a unit vector $k_1 \mathbf{g}_1$ with a phase shift $a_2 k_2$ between adjacent wires, and the same for array 2. The states of equal energy obtained by means of this procedure form straight lines in the 2D BZ. Respectively, the Fermi sea is not a circle with radius k_F like in the case of free 2D gas, but a cross in the k plane bounded by these four lines¹³ (see Fig.2).

Due to the weak inter-wire interaction, the excitations in the 2D BZ depicted in Fig.3 acquire two-dimensionality characterized by the quasimomentum $\mathbf{q} = (q_1, q_2)$. However, in case of interaction, the 2D waves constructed from the 1D plane waves in accordance with the above procedure form an appropriate basis for the description of elementary excitations in QCB, in close analogy with the nearly free electron approximation in conventional crystalline lattices. It is easy to believe that the inter-wire interaction does not completely destroy the above quasimomentum classification of eigenstates, and the 2D reconstruction of the spectrum may be described in terms of wave mixing similarly to the standard Bragg diffraction in a weak periodic potential. Moreover, the classification of eigenstates of non-interacting crossed arrays of 1D wires ("empty superlattice") may be effectively used for the classification of energy bands in a real QB superlattice. Our next task is to construct a complete 2D basis for this empty superlattice.

Excitations in a given wire are described as plane waves $L^{-1/2} \exp(ikx)$ with wave number k and initial dispersion law $\omega(k) = v|k|$ (the array number is temporarily omitted). Each excitation in an "empty superchain" is described by its quasi wavenumber q and a band number s ($s = 1, 2, \dots$). Its wave function has the Bloch-type structure,

$$\psi_{s,q}(x) = \frac{1}{\sqrt{L}} e^{iqx} u_{s,q}(x). \quad (2)$$

We confine ourselves with the first BZ of a superchain, $|q| \leq Q/2$, where the Bloch amplitude $u_{s,q}$ and dispersion law ω_s have the following form:

$$u_{s,q}(x) = \exp \left\{ iQx(-1)^{s-1} \left[\frac{s}{2} \right] \operatorname{sign} q \right\}, \quad (3)$$

$$\omega_s(q) = vQ \left(\left[\frac{s}{2} \right] + (-1)^{s-1} \frac{|q|}{Q} \right). \quad (4)$$

To write down these formulas for a specific array, one should add the array index j to the wave function ψ , Bloch amplitude u , coordinate x , quasimomentum q , periods a and Q of the 1D lattice in real and reciprocal space.

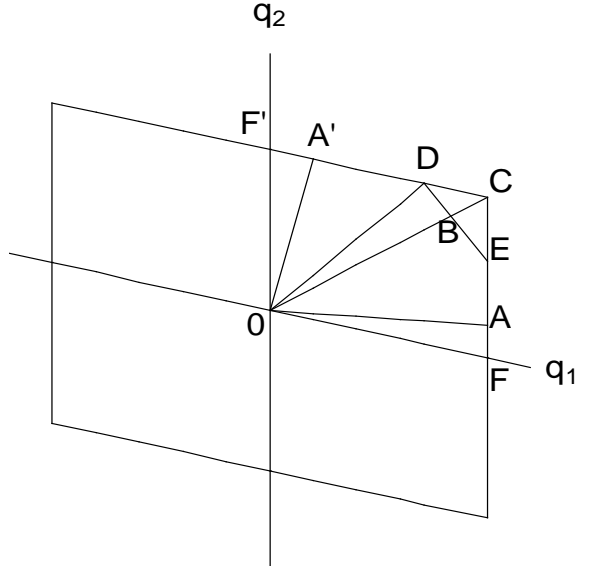


FIG. 3. Two dimensional Brillouin zone of QB. Four polygonal lines along which the dispersion of Bose excitations is calculated in Section V are marked by AOA' , FCF' , and ODE .

The 2D basis of periodic Bloch functions for an empty superlattice is constructed in terms of 1D Bloch functions (2), (3)

$$\Psi_{s,s',\mathbf{q}}(\mathbf{r}) = \psi_{1,s,q_1}(x_1) \psi_{2,s',q_2}(x_2). \quad (5)$$

Here the 2D quasimomentum $\mathbf{q} = (q_1, q_2)$ belongs to the first BZ, $|q_j| \leq Q_j/2$. The corresponding eigenfrequencies are

$$\omega_{ss'}(\mathbf{q}) = \omega_{1,s}(q_1) + \omega_{2,s'}(q_2). \quad (6)$$

We will use this basis in the next section when constructing the excitation spectrum of QB within the reduced band scheme.

The full Hamiltonian of the QB is,

$$H = H_1 + H_2 + H_{int}, \quad (7)$$

where H_j describes the 1D boson field characterised by the parameters v_j, g_j in the j -th array (see eq. (1)), and H_{int} is the interwire interaction. One may neglect interwire tunneling and restrict oneself by the capacitive interaction only, provided the vertical distance d between the wires is substantially larger than the screening radii r_j within the wires. Then

$$H_{int} = V_0 \sum_{n_1, n_2} \int dx_1 dx_2 \Phi \left(\frac{x_1 - n_1 a_1}{r_1}, \frac{n_2 a_2 - x_2}{r_2} \right) \times \partial_{x_1} \theta_1(x_1, n_2 a_2) \partial_{x_2} \theta_2(n_1 a_1, x_2). \quad (8)$$

It stems from the Coulomb interaction between intrawire charge fluctuations within the crossing area. The size of intrawire fluctuations is determined by r_j . The coupling strength is $V_0 = 2e^2/d$, and the function $\Phi(\xi_1, \xi_2)$ is

$$\Phi(\xi_1, \xi_2) = \frac{\zeta_1(\xi_1)\zeta_2(\xi_2)}{\sqrt{1 + |\mathbf{r}_{12}|^2/d^2}} \approx \zeta_1(\xi_1)\zeta_2(\xi_2), \quad (9)$$

provided $|\mathbf{r}_{12}|^2/d^2 \ll 1$. Thus the interaction is separable in this limit.

The above approximation looks realistic for QCB fabricated from carbon nanotubes³. In this case the Coulomb interaction is screened at a distance of the order of the nanotube radius¹⁶ R_0 , therefore $r_{1,2} \sim R_0$. The minimal radius of a single-walled carbon nanotube is about $R_0 = 0.35 \div 0.4 \text{ nm}$ (see¹⁷). The vertical distance d in artificially produced nanotube networks is estimated as $d \approx 2 \text{ nm}^3$. Therefore the ratio $r_0^2/d^2 \approx 0.04$ is really small.

In the quasimomentum representation (5,2,3) the full Hamiltonian (7) acquires the form,

$$H = \frac{\hbar v g}{2} \sum_{j=1}^2 \sum_{s, \mathbf{q}} \pi_{js\mathbf{q}}^+ \pi_{js\mathbf{q}} + \frac{\hbar}{2 v g} \sum_{j'=1}^2 \sum_{s, s', \mathbf{q}} W_{jsj's'\mathbf{q}} \theta_{js\mathbf{q}}^+ \theta_{j's'\mathbf{q}}, \quad (10)$$

where $v = \sqrt{v_1 v_2}$, $g = \sqrt{g_1 g_2}$, while $\sqrt{vg/v_j g_j} \theta_{js\mathbf{q}}$ and $\sqrt{v_j g_j/vg} \pi_{js\mathbf{q}}$ are the Fourier components of the boson fields θ_j and π_j . The matrix elements for interwire coupling are given by:

$$W_{jsj's'\mathbf{q}} = \omega_{js}(q_j) \omega_{j's'}(q_{j'}) [\delta_{jj'} \delta_{ss'} + \phi_{jsj's'\mathbf{q}} (1 - \delta_{jj'})].$$

Here $\omega_{js}(q_j)$ are eigenfrequencies (4) of the “unperturbed” 1D mode pertaining to an array j . The coefficients

$$\phi_{1s2s'\mathbf{q}} = \phi(-1)^{s+s'} \text{sign}(q_1 q_2) \Phi_{1s2s'\mathbf{q}},$$

$$\phi = \frac{g V_0 r_0^2}{\hbar v a}, \quad r_0 = \sqrt{r_1 r_2}, \quad a = \sqrt{a_1 a_2}, \quad (11)$$

are proportional to the dimensionless Fourier component of the interaction strengths

$$\Phi_{1s2s'\mathbf{q}} = \int d\xi_1 d\xi_2 \Phi(\xi_1, \xi_2) e^{-i(r_1 q_1 \xi_1 + r_2 q_2 \xi_2)} \times u_{1,s,q_1}^*(r_1 \xi_1) u_{2,s',q_2}^*(r_2 \xi_2). \quad (12)$$

The Hamiltonian (10) describes a system of coupled harmonic oscillators, and can be *exactly* diagonalized.

The diagonalization procedure is cumbersome in the general case due to mixing of states belonging to different bands and arrays. However, in the case of separable interwire potential (9) one easily comes to a compact secular equation for the eigenfrequencies of QCB:

$$F_{1q_1}(\omega^2) F_{2q_2}(\omega^2) = \frac{1}{\varepsilon}, \quad (13)$$

where

$$F_{jq}(\omega^2) = \frac{r_j}{a_j} \sum_s \frac{\phi_{js}^2(q) \omega_{js}^2(q)}{\omega_{js}^2(q) - \omega^2}, \quad (14)$$

$$\phi_{js}(q) = (-1)^s \text{sign}(q) \int d\xi \zeta_j(\xi) e^{ir_j q \xi} u_{jsq}(r_j \xi),$$

and the dimensionless coupling constant ε can be written as

$$\varepsilon = \left(\phi \frac{a}{r_0} \right)^2 = \left(\frac{g V_0 r_0}{\hbar v} \right)^2 = \left(\frac{2 R_0 g e^2}{d \hbar v} \right)^2. \quad (15)$$

For nanotube QCB, the first factor within parentheses is about 0.35. The second one, that is nothing but the corresponding QCB “fine structure” constant, can be estimated as 0.9 (we used the values of $g = 1/3$ and $v = 8 \times 10^7 \text{ cm/sec}$, see Ref.¹⁸). Therefore $\varepsilon \approx 0.1$, and the coupling is really weak.

III. ENERGY SPECTRUM

Due to weakness of the interaction, the systematics of unperturbed plasmon levels and states is grossly conserved, at least in the low energy region corresponding to the first few bands. This means that perturbed eigenstates could be described by the same quantum numbers as the unperturbed ones. The interband mixing is significant only along the high symmetry directions in the first BZ (BZ boundaries and lines $q_j = 0$). In zeroth approximation with respect to the weak interaction, these lines are determined by the Bragg conditions. Inter-array mixing within the same energy band is strong only for waves with quasimomenta close to the resonant lines in the BZ. In zeroth approximation with respect to the interaction, these lines are determined by the conditions $\omega_{1s}^2(q_1) = \omega_{2s'}^2(q_2)$ with all possible positive integers s, s' . In the rest of the BZ, the initial systematics can be used.

The three next figures illustrate the main features of the excitation spectrum. In Fig.4 the dispersion curves, corresponding to quasi momenta changing along the line AOA' of Fig.3 are plotted in comparison with those for non interacting arrays. (In all figures within this section we use units $\hbar = Q_2 = v_2 = 1$, and $v_1 Q_1 = 1.4$). In what follows we use (j, s) notations for the unperturbed boson propagating along the j -th array in the s -th band. Then the lowest curve in the left part of Fig.4 (line AO in

Fig.3) is, in fact, the slightly renormalized dispersion of a (2, 1) plasmon, the middle curve describes (1, 1) plasmon, and the upper curve is the dispersion of a (1, 2) plasmon. The fourth frequency, corresponding to a (2, 2) plasmon, is far above and is not displayed in this part of the figure. The right part of Fig.4 describes (1, 1) plasmon (lowest curve), (2, 1) plasmon (middle curve) and (2, 2) plasmon (upper curve). It is seen that the dispersion remains linear along the whole line AOA' except at a nearest vicinity of the BZ boundary (see insets in Fig.4). It is clearly seen that the plasmon preserve their 1D character along these lines, and small deviation from linearity is observed only near the boundaries of the BZ. The interband hybridization gaps for bosons propagating along the j -th array can be estimated as $\Delta\omega_{12}^j \sim v_j Q_j \varepsilon r_0/a$.

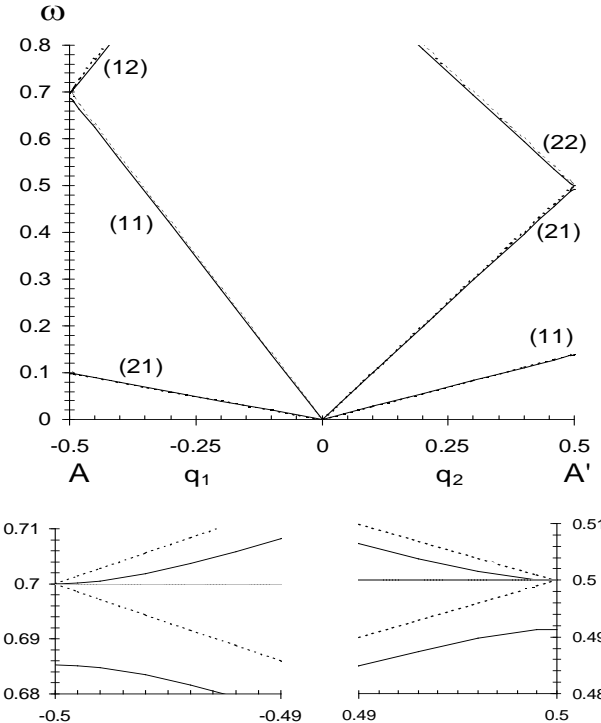


FIG. 4. The energy spectrum of QCB (solid lines) and non-interacting arrays (dashed lines) for quasimomenta at the line AOA' of Fig.3 ($q_2 = 0.2q_1$ along line AO and $q_1 = 0.2q_2$ along line OA'). Insets: Zoomed vicinity of the point $q_1/Q_1 = 0.5$, $\omega = 0.7$ (left side); and the point $q_2/Q_2 = 0.5$, $\omega = 0.5$ (right side).

More pronounced effects of wave mixing are seen in Fig. 5 where the dispersion curves corresponding to the line FCF' (Fig.3) along the boundary of the BZ are plotted. Again, the dispersion laws retain their 1D character along the major part of the boundary. The interaction opens the gap in the 1D bands for arrays 1 and 2 along the lines FC and CF' respectively. Odd (u) and even (g) combinations of two waves are formed as a result of wave mixing. Strong 2D effects are observed around the points D and E . As a result we observe the *dimensional*

crossover $1D \rightarrow 2D$ when moving along the boundary of the Z.

The strongest wave-mixing effects are observed along the line ODE in Fig.3. Here the plasmons belonging to arrays 1 and 2 are mixed along the whole line. They form odd and even combinations but the dispersion is nearly linear everywhere except at the vicinity of the points D and E where *three-wave mixing* takes place. In a square QCB the strong wave-mixing occurs in the vicinity of the diagonals of the BZ¹⁵.

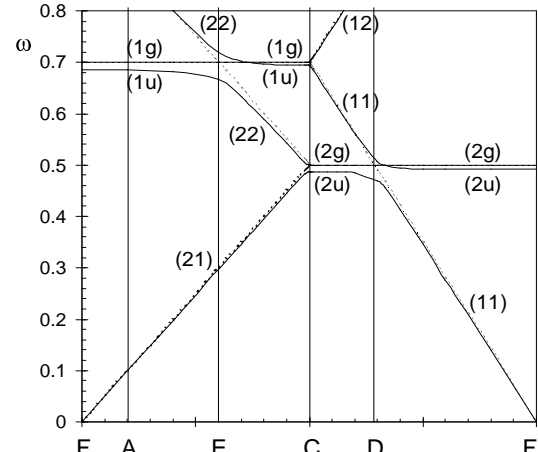


FIG. 5. The energy spectrum of QCB (solid lines) and noninteracting arrays (dashed lines) for quasimomenta at the boundary of the BZ (line FCF' in the Fig.3)

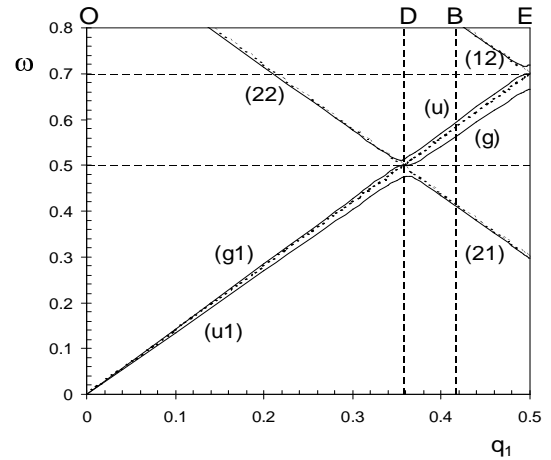


FIG. 6. The energy spectrum of QCB (solid lines) and non-interacting arrays (dashed lines) for quasimomenta at the resonant line of the BZ (line ODE in Fig.3)

The low-energy part of the spectrum along most part of the line OD is described by the secular equation

$$\prod_{j=1}^2 \left(\frac{\varphi_j^2(q_j)\omega^2}{\omega_j^2(q_j) - \omega^2} + F_j \right) = \frac{1}{\varepsilon}, \quad (16)$$

which follows from the general equation(14). Its solution gives two nearly linear plasmon bands which conserve their LL character in spite of the $2D$ wave mixing. Just this solution is described by eq. (3.10) of Ref.⁸. So, our exact procedure confirms the conclusion of renormalization approach of this paper that the sliding LL phase may exist in two-dimensional QCB, and the inter-array density-density interaction is irrelevant for the LL fixed point.

Finally we show the lines of equal frequency for Bose excitations (Figs. 7,8). These lines should be compared with the Fermi surface "cross" shown in Fig. 2. Their rounding near the broken line ODE is a manifestation of $1D \rightarrow 2D$ crossover. Similar rounding of the $1D$ Fermi surface due to inter-array tunneling was discussed in Ref.¹⁴.

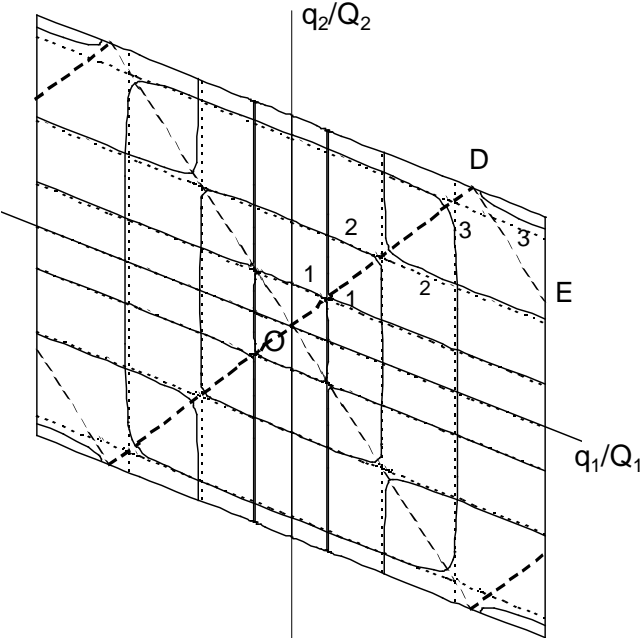


FIG. 7. The lines of equal frequency for QCB (solid lines) and noninteracting arrays (dashed lines). The lines 1, 2, 3 correspond to the frequencies $\omega_1 = 0.1$, $\omega_2 = 0.25$, $\omega_3 = 0.45$.

IV. CORRELATIONS AND OBSERVABLES

The correlation functions of QCB in the infrared limit are usually discussed in a framework of the theory of sliding LL phases⁸. These are the Drude peak in the optical conductivity, $\sigma(\omega) = D(T)\delta(\omega)$, the power-low temperature dependence of resistivity, and the crossover from isotropic to anisotropic conductivity at a certain length scale, when the current is inserted at a point on array 1 and extracted at another point on array 2. All these features are reproduced by our exact solution which generates the LL thermodynamics and transport as an intrinsic property of QCB Hamiltonian (10).

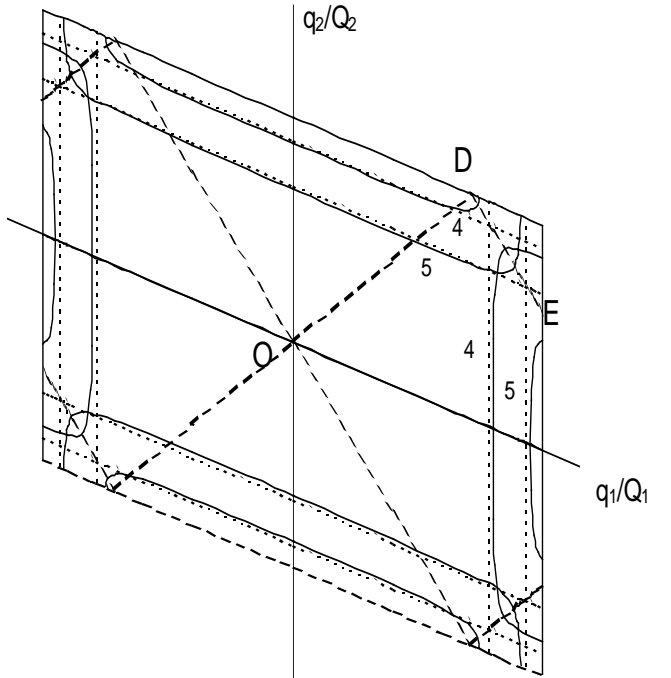


FIG. 8. The lines of equal frequency for QCB (solid lines) and noninteracting arrays (dashed lines). The lines 4, 5 in the lower panel correspond to the frequencies $\omega_4 = 0.55$, $\omega_5 = 0.65$

In this section we discuss in brief the correlation properties which allow one to reveal specific $2D$ features of QCB at *finite frequency and momentum*. One of the main effects specific for a QCB is the appearance of non-zero transverse momentum-momentum correlation function. In space-time coordinates (\mathbf{x}, t) it reads,

$$G_{12}(\mathbf{x}, t) = \langle [\pi_1(x_1, 0; t), \pi_2(0, x_2; 0)] \rangle. \quad (17)$$

This function describes the momentum response at the point $(0, x_2)$ of the second array at time t caused by initial ($t = 0$) perturbation at the point $(x_1, 0)$ of the first array. Standard calculations lead to the following expression,

$$G_{12}(\mathbf{x}; t) = -i \frac{V_0 r_0^2}{4\pi^2 \hbar} \int_{-\infty}^{\infty} dk_1 dk_2 \phi_1(k_1) \phi_2(k_2) k_1 k_2 \times \times \sin(k_1 x_1) \sin(k_2 x_2) \frac{v_2 k_2 \sin(v_2 k_2 t) - v_1 k_1 \sin(v_1 k_1 t)}{v_2^2 k_2^2 - v_1^2 k_1^2}, \quad (18)$$

where $\phi_j(k)$ is the Fourier component (14) written in the extended BZ.

This correlator is shown in Fig. 9. Here the non-zero response corresponds to the peak located at the line determined by the obvious kinematic condition $|x_1| + |x_2| = vt$. The finiteness of the interaction radius slightly spreads this peak and changes its profile.

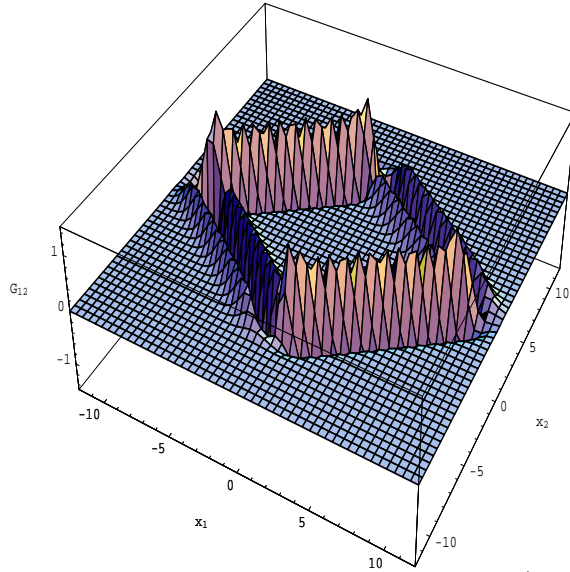


FIG. 9. The transverse correlation function $G_{12}(x_1, x_2; t)$ for $r_0 = 1$ and $vt = 10$

Further manifestation of the 2D character of QCB is related to a periodic energy transfer between the two arrays of wires. Consider an initial perturbation which, in the system of *non*-interacting arrays, excites a plane wave propagating within the first array along the \mathbf{e}_1 direction,

$$\begin{aligned} \langle \theta_1(x_1, n_2 a_2; t) \rangle &= \frac{\rho_0}{\sqrt{2}|q_1|} \sin(q_1 x_1 + q_2 n_2 a_2 - v_1 |q_1| t), \\ \langle \theta_2(n_1 a_1, x_2; t) \rangle &= 0, \end{aligned} \quad (19)$$

(ρ_0 is the charge density amplitude). If the wave vector \mathbf{q} , satisfying the condition $|\mathbf{q}| \ll Q_{1,2}/2$, is not close to the resonant line of the first BZ, weak interwire interaction $\phi = \epsilon r_0/a$ slightly changes the $\langle \theta_1 \rangle$ component and leads to the appearance of a small $\langle \theta_2 \rangle \sim \phi$ component. But for \mathbf{q} lying on the resonant line ($v_1 |q_1| = v_2 |q_2| \equiv \omega_{\mathbf{q}}$), both components within the main approximation have the same order of magnitude

$$\begin{aligned} \theta_1(x_1, n_2 a_2; t) &= \frac{\rho_0}{\sqrt{2}|q_1|} \cos\left(\frac{1}{2}\phi_{\mathbf{q}}\omega_{\mathbf{q}}t\right) \times \\ &\quad \sin(q_1 x_1 + q_2 n_2 a_2 - \omega_{\mathbf{q}}t), \end{aligned} \quad (20)$$

$$\begin{aligned} \theta_2(n_1 a_1, x_2; t) &= \frac{\rho_0}{\sqrt{2}|q_1|} \sin\left(\frac{1}{2}\phi_{\mathbf{q}}\omega_{\mathbf{q}}t\right) \times \\ &\quad \cos(q_1 n_1 a_1 + q_2 x_2 - \omega_{\mathbf{q}}t). \end{aligned} \quad (21)$$

Here $\phi_{\mathbf{q}} \equiv \phi_{1121\mathbf{q}}$ (see Eq.(11)). This corresponds to a 2D propagation of a plane wave with wave vector \mathbf{q} , *modulated* by a “slow” frequency $\sim \phi\omega$. As a result, an energy is periodically transferred from one array to another during a long period $T \sim (\phi\omega)^{-1}$ (see Fig.10). These peculiar “Rabi oscillations” may be considered as one of the fingerprints of the physics exposed in QCB systems.

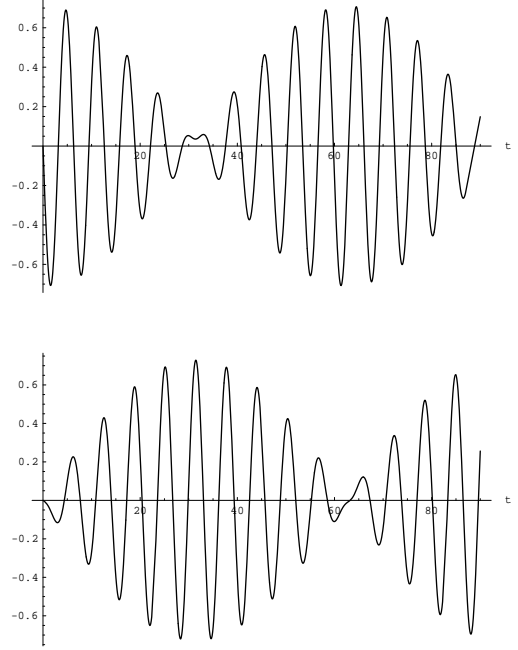


FIG. 10. Periodic energy exchange between arrays (“Rabi oscillations”)

Interarray interaction affects also the optical conductivity $\sigma(\omega)$. It was shown in Ref.¹⁵ that as a result a transverse component $\sigma_{\perp}(\omega)$ appears.

V. CONCLUSION

We have shown that the bosonization procedure may be applied to the Hamiltonian of 2D quantum grids at least in the first few Brillouin zones. The energy spectrum of QCB shows the characteristic properties of LL at $|\mathbf{q}|, \omega \rightarrow 0$, but at finite \mathbf{q} , the density and momentum waves may have either 1D or 2D character depending on the direction of the wave vector. Due to interwire interaction, unperturbed states, propagating along the two arrays are always mixed, and transverse components of correlation functions do not vanish. For quasi-momenta near the diagonal of the BZ, such mixing is strong, and the transverse correlators possess specific dynamical properties.

¹ J. Voit, Rep. Prog. Phys. **58**, 977 (1994).

² P. W. Anderson, Science **235**, 1196 (1987).

³ T. Rueckes, K. Kim, E. Joselevich, G. Y. Tseng, C. L. Cheung, and C. M. Lieber, Science **289**, 94 (2000).

⁴ J. von Delft, and H. Schoeller, Ann. der Physik **7**, 225 (1998).

⁵ X. G. Wen, Phys. Rev. B**42**, 6623 (1990); H. J. Schultz, Int. J. Mod. Phys. **1/2**, 57 (1991).

⁶ V. Emery, E. Fradkin, S. A. Kivelson, and T.C. Lubensky, Phys. Rev. Lett. **85**, 2160 (2000).

⁷ A. Vishwanath and D. Carpentier, Phys. Rev. Lett. **86**, 676 (2001).

⁸ R. Mukhopadhyay, C. L. Kane, and T. C. Lubensky, Phys. Rev. B **63**, 081103(R) (2001); Phys. Rev. B **64**, 045120 (2001); cond-mat/0102163.

⁹ C. S. Hern, T. C. Lubensky, and J. Toner, Phys. Rev. Lett. **83**, 2745 (1999).

¹⁰ S. L. Sondhi and K. Yang, Phys. Rev. B**63** 054430 (2001); C. L. Kane, R. Mukhopadhyay, and T. C. Lubensky, Phys. Rev. Lett. **88**, 036401 (2002).

¹¹ J. E. Avron, A. Raveh, and B. Zur, Rev. Mod. Phys. **60**, 873 (1988).

¹² Y. Avishai, and J. M. Luck, Phys. Rev. B**45**, 1074 (1992).

¹³ F. Guinea, and G. Zimanyi, Phys. Rev. B **47**, 501 (1993).

¹⁴ A. H. Castro Neto, and F. Guinea, Phys. Rev. Lett. **80**, 4040 (1998).

¹⁵ I. Kuzmenko, S. Gredeskul, K. Kikoin and Y. Avishai, Low Temp. Phys. **28**, No.8/9 (2002).

¹⁶ K. Sasaki, cond-mat/0112178.

¹⁷ S. G. Louie in *Carbon Nanotubes*, M. S. Dresselhaus, G. Dresselhaus, and Ph. Avouris (Eds.), Springer, Berlin 2001 [Topics Appl. Phys. **80**, 113 (2001)].

¹⁸ R. Egger, A. Bachtold, M. S. Fuhrer, M. Bockrath, D. H. Cobden, and P. L. McEuen, cond-mat/0008008.